Atmos. Chem. Phys. Discuss., 12, 12623–12662, 2012
www.atmos-chem-phys-discuss.net/12/12623/2012/
doi:10.5194/acpd-12-12623-2012

Atmospheric Chemistry and Physics Discussions

Time dependence of immersion freezing

A. Welti[1], **F. Lüönd**[1,2], **Z. A. Kanji**[1], **O. Stetzer**[1], **and U. Lohmann**[1]

[1]ETH Zurich, Institute for Atmospheric and Climate Science, Switzerland
[2]Federal Office of Metrology, Bern, Switzerland

Received: 26 April 2012 – Accepted: 27 April 2012 – Published: 16 May 2012

Correspondence to: A. Welti (andre.welti@env.ethz.ch)

Published by Copernicus Publications on behalf of the European Geosciences Union.

Abstract

The time dependence of immersion freezing was studied for temperatures between 236 K and 243 K. Droplets with single immersed, size-selected 400 nm and 800 nm kaolinite particles were produced at 300 K, cooled down to supercooled temperatures typical for mixed-phase cloud conditions, and the fraction of frozen droplets with increasing residence time was detected. To simulate the conditions of immersion freezing in mixed-phase clouds we used the Zurich Ice Nucleation Chamber (ZINC) and its vertical extension, the Immersion Mode Cooling chAmber (IMCA). We observed that the frozen fraction of droplets increased with increasing residence time in the chamber. This suggests that there is a time dependence of immersion freezing and supports the importance of a stochastic component in the ice nucleation process. The rate at which droplets freeze was observed to decrease towards higher temperatures and smaller particle sizes. Comparison of the laboratory data with four different ice nucleation models, three based on classical nucleation theory with different representations of the particle surface properties and one singular, suggest that the classical, stochastic approach combined with a distribution of contact angles is able to reproduce the ice nucleation observed in these experiments most accurately. Using the models to calculate the increase in frozen fraction at typical mixed-phase cloud temperatures over an extended period of time, yields an equivalent effect of −1 K temperature shift and an increase in time scale by a factor of ∼10.

1 Introduction

The formation of ice crystals in supercooled clouds is usually initiated on the surface of aerosol particles. An important class of ice nucleating particles (IN) are mineral dust aerosols blown off from arid surfaces (Kumai, 1951; Isono et al., 1959; DeMott et al., 2003; Eastwood et al., 2008).

ACPD
12, 12623–12662, 2012

Mixed phase clouds containing liquid droplets and ice crystals cover about 15.3 % of the globe with the highest occurrence in mid-latitudes and over the polar oceans (Wang et al., 2010). One pathway of ice crystal formation in these clouds is by aerosol particles acting as cloud condensation nuclei (CCN) at temperatures above 273 K, cooling of the cloud droplets and subsequent nucleation of ice at a certain degree of supercooling. If ice formation is heterogeneously initiated on the aerosol surface the process is referred to as immersion freezing. This is the dominant freezing mechanism down to a supercooling of approximately 235 K below which homogeneous freezing within the droplet volume becomes the more efficient mode of ice nucleation (Pruppacher and Klett, 1997). Other ice nucleation modes like deposition nucleation, condensation- and contact freezing (Vali, 1985) can also be active in mixed phase clouds but are thought to be only of minor importance because they require dry unimmersed aerosols to be present.

The efficiency of ice formation in mixed-phase clouds and the transformation of small cloud droplets to larger ice crystals that precipitate, influences the surface water distribution, e.g. the freezing of liquid water droplets in mixed-phase clouds is one of the essential processes for precipitation formation in mid latitudes (Houghton, 1950).

The change in the cloud brightness resulting from the freezing of cloud droplets has an effect on the Earth's surface energy budget (Cantrell and Heymsfield, 2005; Lohmann, 2002). In addition to freezing of droplets, the radiative properties are influenced by the depletion of liquid water via the Bergeron-Findeisen process in partially glaciated clouds (Westbrook and Illingworth, 2009).

Further, time dependence of ice formation is also of interest because of its influence on chemical reactions, which occur on the surface of cloud droplets. In summary, many major mixed-phase cloud characteristics (light scattering, precipitation formation, chemistry) depend on the size of the cloud droplets, which in turn is linked by the Bergeron-Findeisen process to the rate at which ice nucleates in the interior of the supercooled cloud droplets (Tabazadeh et al., 2002).

ACPD
12, 12623–12662, 2012

To predict the radiative properties and precipitation development of mixed-phase clouds, a detailed understanding of the mechanisms by which droplets freeze is paramount. In particular, the question of whether the fraction of ice and liquid water depends on time or solely on temperature has not been answered definitively by experiments.

Two theories of immersion freezing have been discussed since the 1950's. First, the stochastic hypothesis formulated by Bigg (1953) which is based on the concept that, within supercooled water, thermal fluctuations of water molecules can produce clusters which resemble the structure of ice. By capturing and losing molecules, some of these ice germs grow to a size (characterised by the critical radius) where they become stable and initiate freezing. The number of molecules required to form a stable ice germ within a droplet decreases with decreasing temperature and therefore increases the probability of critical germ formation. Subsequent freezing of a droplet and development of the macroscopic ice crystal takes place at the ice-water interface of the first critical germ. The presence of a particle surface in a supercooled droplet reduces the amount of water molecules that are needed to reach the stable cluster radius by allowing the germ to form on it as a spherical cap. The number of critical ice germs forming per unit time and unit surface area of the IN is referred to as the nucleation rate. This stochastic approach is known as the classical nucleation theory (CNT).

The second, singular hypothesis, proposed by Langham and Mason (1958) assumes that at a given supercooling, the radius of ice germ forming on the aerosol surface is determined by surface features, and thermal fluctuations have negligible influence on the ice germ radius. If this radius is larger than the critical germ radius at the given supercooling, the droplet freezes immediately. Otherwise the droplet will stay liquid irrespective of the time during which the droplet is exposed to the given supercooling.

Experimental support for both a stochastic and a singular component in immersion freezing has been found. A time dependence of ice nucleation was observed and described by Vonnegut (1949) and has been supported by a number of consecutive cloud chamber studies, mainly on AgI (e.g., Fletcher, 1959; Wartburton and Heffernan, 1964).

ACPD
12, 12623–12662, 2012

Recent cold stage experiments which investigated the repeated exposure of the same sample to low temperatures (Koop, 2004; Shaw et al., 2005; Vali, 2008; Murray et al., 2011; Broadley et al., 2012) and differential scanning caliometry (DSC) of oil/water emulsion samples (Zobrist et al., 2007; Marcolli et al., 2007; Pinti et al., 2012), found evidence of varying onset freezing temperatures when measurements where repeated with the same sample. This supports the stochastic approach. On the other hand experiments with a large number of droplets that contain nuclei as performed in cloud- or diffusion chambers (Niedermeier et al., 2011; Connolly et al., 2009), observed a more singular freezing behaviour. In the cold stage study of Vali and Stansbury (1966) it was concluded that neither a purely stochastic nor a singular description is applicable to represent the probability of ice nucleation at a constant temperature.

To represent ice nucleation in numerical climate models accurately it is useful to know which hypothesis is suitable for a certain particle population.

The current study uses the same experimental setup as was used by Lüönd et al. (2010) to investigate the size dependence of immersion freezing on kaolinite particles. The measurements reported by Lüönd et al. (2010) were done at a constant residence time in the supercooled region of the experiment. Fitting the experimental data with either a stochastic or singular model revealed a comparable difference of the fit curves from the measurements. They proposed that time-dependent measurements could help assess the differences and applicability of the two approaches in representing immersion freezing. In the present study we approached the nature of the time-dependence in immersion freezing by measuring the frozen fraction of a large number of droplets containing single immersed particles at different residence times while keeping the experimental temperature constant. In a second step described in Sect. 4, we tested a stochastic, a singular and two modified-stochastic model formulations for their ability to represent the measured data. Based on the best fit of each model we then calculated the glaciation state of a mixed-phase cloud after 30 min at a constant temperature, which corresponds to a typical time step in a global climate model. To simplify the experimental findings for climate models, we derived apparent,

ACPD
12, 12623–12662, 2012

temperature dependent contact angles that might incorporate the non-stochastic component of freezing in an otherwise purely stochastic formulation. Such a formulation might be useful for climate models due to its relative simplicity. In addition, we calculated the median freezing temperature as a function of the surface area of the aerosol for the four models.

2 Experimental method

The Zurich Ice Nucleation Chamber (ZINC) (Stetzer et al., 2008), a parallel plate continuous flow diffusion chamber (CFDC) following the working principle first described by Rogers (1988) with the vertical extension Immersion Mode Cooling chAmber (IMCA) (Lüönd et al., 2010) was used to study the time dependence of immersion freezing. A schematic of the experimental setup is shown in Fig. 1. The IMCA/ZINC combination allows to mimic a quasi-realistic pathway of immersion freezing by activating the aerosol as CCN at temperatures above 273 K, cooling the droplets down to supercooled temperatures and investigate immersion freezing at constant temperatures and at water saturated conditions for the residence time in the ZINC chamber. The constant temperature and saturation conditions in ZINC represent conditions of a static mixed-phase cloud.

The frozen fraction of droplets containing single immersed kaolinite particles was detected with the Ice Optical DEpolarization detector (IODE) described in Nicolet et al. (2010).

2.1 Aerosol generation and droplet activation

Kaolinite (Fluka) particles were aerosolised in a Fluidized Bed Aerosol Generator (TSI Model 3400A) and size selected according to their electrostatic mobility with a Differential Mobility Analyser (DMA, TSI Model 3081). To confine the size distribution of the aerosol generated by the fluidized bed aerosol generator, a cascade of two cyclones

ACPD
12, 12623–12662, 2012

and two parallel operated impactors were introduced into the particle stream before the DMA (not shown in Fig. 1). The resulting removal of large particles ensures a minimum contribution from multiple charged particles to the selected aerosol size for the experiments. Moreover, it has been shown in the study of Welti et al. (2009), that the selected sizes of 400 nm and 800 nm are in the downslope of the size distribution produced by the aerosol generator, so the contribution of larger double or triple charged particles with an equal electrical mobility diameter is below 10 %.

The size selected aerosol is sampled by the IMCA chamber. The inner walls of IMCA are lined with wet filter paper, and a horizontal and vertical temperature gradient is applied to generate water supersaturation at high temperatures in the top part and water saturation at its bottom at temperatures close to the experimental freezing temperatures applied in ZINC. In the top part of IMCA the mineral particles act as CCN at 300 K and supersaturations up to 20 %. Along their travel through IMCA, the particles which are now immersed in droplets, are cooled down to the experimental temperature applied in ZINC.

2.2 Freezing experiments

In the ZINC chamber the droplets are exposed to freezing temperatures between 236 K and 244 K which are atmospherically relevant glaciation temperatures for mixed-phase clouds as supercooled cloud droplets can exist down to approximately 235 K (Pruppacher and Klett, 1997). The uncertainty in the reported temperature is on the order of ±0.3 K, mainly determined by the temperature gradient across the sample layer. The aerosol sample is sandwiched between two layers of particle free sheath-air to control its width and lateral position between the walls. The front and back wall of ZINC are covered with an ice layer and held at two different temperatures to generate water saturation at the sample position. The water saturated conditions prevent evaporation or condensation of the droplets which ensures that the droplet temperature is very close to the air temperature.

ACPD
12, 12623–12662, 2012

The temperature and saturation conditions at the sample position between the warm and the cold wall of ZINC are calculated from the wall temperature difference and the fact that the water vapour pressure at both walls equals the saturation vapour pressure of ice at the respective temperature.

Figure 2 shows the temperature and saturation condition in the sample layer for one example experiment at 240 K and a flow velocity of 5 l min^{-1} in IMCA and 10 l min^{-1} in ZINC. Technical details on IMCA and ZINC can be found in the work of Lüönd et al. (2010) and Stetzer et al. (2008), respectively.

To investigate the effect of time on immersion freezing, the IODE detector was mounted at four different positions (indicated in Fig. 1) on the ZINC chamber and three different flow conditions given in Table 1 were applied to alter the residence time of the supercooled droplets within the ZINC chamber. Detecting the frozen fraction with the IODE detector (see Sect. 2.4) at the four positions of ZINC allowed us to pursue the evolution of the fraction of frozen droplets as a function of residence time at constant temperatures.

Residence time was counted starting from stable temperature and saturation conditions in ZINC as indicated in Fig. 2. The droplets are exposed to supercooled temperatures already before they reach stable conditions. In this transition, freezing of some droplets is initiated. But as the prevailing temperatures are above or close to the observed onset temperature of immersion freezing, we expect the contribution to the total frozen fraction to be only minor. Detection positions 1–3 are located at the freezing section of ZINC, whereas detection port 4 is at the beginning of the evaporation section. As can be seen from Fig. 2, temperature and relative humidity change in the transition from the freezing to the evaporation section. This might cause a small systematic bias in the reported frozen fraction towards lower ratios at position 4.

2.3 Modifications of the experimental setup as compared to Lüönd et al. (2010)

In the transition between IMCA and ZINC asymmetric additional sheath air is introduced to counteract the displacement of the sample layer towards the cold wall due

ACPD
12, 12623–12662, 2012

to the superposition of the laminar and the buoyant flow created by the temperature gradient in ZINC. The addition of a higher flow of sheath air on the cold side counters the buoyant displacement and ensures that the sample flow remains in the centre of ZINC where the ice-water fraction can be detected by the IODE detector. Figure 3 shows a Fluent simulation of the flow velocity profile in the transition region from IMCA to ZINC where the additional sheath air is introduced. An additional advantage of this improvement is, that IMCA and ZINC can be operated at different total flow rates i.e. a low flow in IMCA to increase the drop growth time and adjustable higher flow-rates in ZINC to vary the residence time for ice nucleation (cf. Table 1).

2.4 Detection and discrimination of droplets and ice

To detect the fraction of liquid droplets and ice crystals, the depolarization detector IODE (Nicolet et al., 2010) was used. Linearly polarized laser light is aligned to the sample layer passing through ZINC. Frozen droplets are known to depolarize polarized light, especially if they develop an aspherical shape, whereas liquid droplets do not. The intensity of light backscattered by the frozen and unfrozen droplets is split into its components parallel and perpendicular to the incident polarization by a Wollaston prism and the depolarization is registered. Experiments were repeated up to seven times and average values are reported. For each measurement the background signal of the IODE detector was determined and subtracted. The background signal stems from reflections in ZINC, internal reflections within IODE and eventually inactivated, dry aerosol particles. It has been reported in Lüönd et al. (2010) that the latter do not generate a signal sufficiently strong to be counted by the peak detection algorithm. More details about the components and functionality of IODE or signal analysis can be found in the work of Nicolet et al. (2010) and Lüönd et al. (2010).

ACPD
12, 12623–12662, 2012

3 Immersion freezing results

Size selected, single immersed kaolinite particles have been tested for their ice nucleation efficiency by measuring the temperature dependent frozen fraction for variable residence times. Generally the frozen fraction of droplets containing similar sized kaolinite particles increases towards the homogeneous freezing temperature. This is likely due to the decreasing radius of the critical ice embryo, thus with a higher probability of stable germ formation. Variations in the surface features of the individual particles which catalyse the formation of a critical ice embryo cause a distribution in the nucleation activity at a given temperature. The rather steep increase in the temperature dependent frozen fraction as shown in Fig. 4 indicates the small temperature range over which immersion freezing on this type of kaolinite becomes efficient.

3.1 Size dependence

Figure 4 shows an example of the detected frozen fraction for two sets of measurements with 400 nm and 800 nm kaolinite particles at a constant residence time of 9 s. The non-averaged, single-measurement data is shown here to illustrate the dataset from which average values where obtained to compute the fit parameters for the different models (cf. Sect. 4.1). From the single-measurement data the influence of particle size on the onset temperature and frozen fraction at a specific temperature of immersion freezing can be seen. Smaller kaolinite particles tend to be significantly less efficient IN, especially at higher temperatures. The temperature region where immersion freezing on kaolinite particles is active is close to the homogeneous freezing temperature. Compared to homogeneous freezing however, immersion freezing has a gentler slope in the frozen fraction. This indicates a temperature dependent increase in the reduction of the energy barrier to ice nucleation. This thought will be addressed again in Sect. 6.1.

ACPD
12, 12623–12662, 2012

3.2 Time dependence

The averaged, time-dependent dataset is shown in Fig. 5. One data point represents the frozen fraction obtained from the depolarisation measurements of up to 10 000 single detected droplets/ice crystals. We observe a time dependent behaviour of the frozen fraction of the immersion freezing process i.e. the frozen fraction increases with increasing residence time in the ZINC chamber. The steepest increase can be observed for short residence times at low temperatures. Warmer temperatures cause a slower but steady increase in the frozen fraction. From the comparison of the two datasets (400 and 800 nm) shown in Fig. 5, not only a dependency on the experimental temperature but also a relationship between the surface area and freezing time is observed. In the investigated temperature range, smaller surface areas lead to a stronger dependency on nucleation time i.e. the change in frozen fraction over the residence time in the experiment was larger for the 400 nm particles. This is in agreement with the work of Gerber (1976) who found that on AgI particles the time dependence of immersion freezing was reduced when the particle size was increased. In summary, we observe immersion freezing to be dependent on temperature, IN surface and time and therefore at least partly a stochastic phenomena.

4 Analysis of the experimental data with theoretical models

The stochastic and the singular hypotheses discussed in Sect. 1 can be used to derive theoretical fit functions to the experimental results. By testing if the models can reproduce the experimentally measured frozen fraction as a function of temperature, particle size and time accurately, we aim to determine whether one of the concepts is capable to describe the microphysics of immersion freezing. In addition, numerical climate models reached a stage where they are able to incorporate physical representations of the immersion freezing process (e.g., Hoose et al., 2010). Information on what type

ACPD
12, 12623–12662, 2012

of formalism is appropriate to describe heterogeneous ice formation in a cloud, will therefore become of interest for modelling studies.

4.1 Parameterisation of the particle surface

Following the method described in Lüönd et al. (2010), we test four different approaches to parameterise the particle surfaces for their capability to describe the measured time dependence of immersion freezing. Each model is applied to the combined dataset of 400 nm and 800 nm particles. In doing so the obtained fit-parameters are independent of the particle size and represent physical properties of kaolinite particles. One set of parameters is therefore sufficient to derive the frozen fraction of any particle size and temperature. To simplify the analysis of the measurements, the particles are considered to be spherical. With this assumption, the true surface area of the particles is underestimated to some extent.

The four models are summarized in Sects. 4.2 to 4.3. A more detailed discussion of the four approaches can be found in Lüönd et al. (2010).

4.2 Classical nucleation theory based models

Classical nucleation theory is a stochastic approach to describe ice nucleation. CNT assumes that incipient ice clusters are continuously forming and disappearing with a temperature dependent frequency (Barnes et al., 1962). For heterogeneous nucleation, it predicts a probability per unit time and surface area for an ice cluster to reach critical size and initiate the freezing process. According to classical nucleation theory as for example formulated by Bigg (1953) or Fletcher (1969), the probability of occurrence of nucleation events can be described by heterogeneous nucleation rates calculated as

$$J(T,\alpha) = \frac{kT}{h}\exp\left(-\frac{\Delta F_{\mathrm{diff}}(T)}{kT}\right)\cdot n\exp\left(-\frac{\Delta G(T) f_{\mathrm{het}}(\alpha)}{kT}\right) \quad (1)$$

ACPD
12, 12623–12662, 2012

where k is the Boltzmann constant, h Planck's constant, n the number density of water molecules at the interface of the IN with the surrounding liquid and T is temperature. In the case of immersion freezing, the Gibbs free energy for the transfer of water molecules to the ice phase for the critical ice embryo formation is given by

$$\Delta G(T) = \frac{16\pi}{3} \frac{V_{\mathrm{ice}}^2(T)\sigma_{\mathrm{i/w}}^3(T)}{[kT \ln S_i(T)]^2}, \quad (2)$$

where $V_{\mathrm{ice}}(T)$ denotes the volume of a water molecule in the ice embryo and $\sigma_{\mathrm{i/w}}(T)$ is the specific interfacial free energy (also called surface tension) between the ice embryo surface and the surrounding water droplet. S_i is the ice saturation ratio which for immersion freezing is equal to the temperature dependent ratio of the saturation vapour pressure over water and ice.

The compatibility factor which describes the reduction in the free energy barrier as a function of the contact angle α (Chakraverty and Pound, 1964; Pruppacher and Klett, 1997) is

$$f_{\mathrm{het}}(\alpha) = (2 + \cos\alpha)(1 - \cos\alpha)^2/4 \quad (3)$$

The formulas used to derive contact angles from the experimentally measured frozen fraction are summarized in the following Sects. 4.2.1 to 4.2.3. The complexity of the surface parameterisation increases from the purely stochastic, to α-pdf and further to the active site model. The resulting contact angle distributions are shown in Fig. 6. The diffusion energy barrier of a water molecule to cross the water/ice embryo interface is

$$\Delta F_{\mathrm{diff}}(T) = \frac{\partial \ln D_l(T)}{\partial T} kT^2, \quad (4)$$

where $D_l(T)$ denotes the diffusivity of water. As $\Delta F_{\mathrm{diff}}(T)$ is difficult to approach experimentally the parameterisation proposed in the work of Zobrist et al. (2007) is used.

ACPD
12, 12623–12662, 2012

4.2.1 Stochastic model

The particle surface is assumed to be smooth, uniform and equal for all particles. The free fitting parameter is the contact angle α which applies to all particles. A contact angle of 0° reflects epitaxial ice formation whereas 180° represents purely homogeneous nucleation. The frozen fraction is given by

$$f_{\mathrm{i,\,stoch}} = 1 - \exp(-J(T,\alpha)4\pi r_{\mathrm{N}}^2 t_{\mathrm{ZINC}}). \quad (5)$$

where r_{N} is the radius of the IN and t_{ZINC} is the residence time in the ZINC chamber. By minimizing the sum of square error between the experimentally measured frozen fraction and the frozen fraction calculated by Eq. (5) the best fitting contact angle can be derived.

4.2.2 α-pdf model

The contact angle probability density function (α-pdf) approach takes into account the heterogeneity of individual particles in the sample. The particle surface is smooth and uniform for each particle but differs within an ensemble i.e. the contact angle α differs among the particle population.

The distribution of the contact angle occurrence among the particles of a population is assumed to be represented by a log-normal probability density function, given by

$$p(\alpha) = \frac{1}{\alpha\sqrt{2\pi\sigma^2}} \exp\left(-\frac{(\ln(\alpha)-\mu)^2}{2\sigma^2}\right), \quad (6)$$

where μ is the mean contact angle and σ^2 is the variance. The frozen fraction for a given temperature can then be calculated as

$$f_{\mathrm{i},\alpha-\mathrm{pdf}} = 1 - \int_0^{\pi} p(\alpha)\cdot\exp(-J(T,\alpha)4\pi r_N^2 t_{\mathrm{ZINC}})d\alpha. \quad (7)$$

ACPD
12, 12623–12662, 2012

Fit parameters μ and σ are found by minimizing the sum of square errors of Eq. (7) with respect to the experimental data.

4.2.3 Active site model

The active site model takes into account that even the surface of individual particles might vary significantly with respect to their mineralogical surface composition and morphology. Therefore, instead of having a smooth surface, the model assumes that the aerosol is covered with surface inhomogeneities (active sites). A random distribution of active sites is assumed, each having an area of $A_{\alpha_i} = 6\,\mathrm{nm}^2$ over the whole surface of each individual particle. $6\,\mathrm{nm}^2$ corresponds to the cross-sectional area of a critical embryo at 239 K (Lüönd et al., 2010). Each active site is assigned a contact angle. The surface density of contact angle values is defined according to Marcolli et al. (2007) by:

$$\rho(\alpha) = b \cdot \exp\left(\frac{-\beta_1}{\alpha - \beta_2}\right), \tag{8}$$

where b, β_1 and β_2 are free fit parameters.

The freezing probability of one droplet (index j) with one immersed particle during the residence time t_{ZINC} is calculated as one minus the probability that none of the randomly assigned active sites on the particle causes freezing, i.e.

$$p_{\mathrm{frz},j}(T) = 1 - \prod_{i=1}^{m} \exp(-J(T,\alpha_i)\, A_{\alpha_i,j}\, t_{\mathrm{ZINC}}) \tag{9}$$

where m is the number of intervals of contact angles from $[0,\pi]$ (Lüönd et al., 2010). The frozen fraction of an ensemble of particles is then given by

$$f_{\mathrm{i,AS}} = \frac{1}{N_{\mathrm{tot}}} \sum_{j=1}^{N_{\mathrm{tot}}} p_{\mathrm{frz},j}(T). \tag{10}$$

ACPD
12, 12623–12662, 2012

The parameters of $\rho(\alpha)$ is derived by minimizing the sum of the square errors between measurements and the function given in Eq. (10).

4.3 Singular model

The time-independent, singular or deterministic model as proposed in the work of Connolly et al. (2009) describes ice nucleation on active sites which become active at distinct temperatures. This approach is not based on CNT. The frozen fraction of droplets $f_{\mathrm{i,sing}}$ is given by

$$f_{\mathrm{i,sing}} = 1 - \exp(-n_{\mathrm{s}}(T) \cdot 4\pi r_{\mathrm{N}}^2), \tag{11}$$

where $n_{\mathrm{s}}(T)$ denotes the surface density of sites active at a given temperature. To fit Eq. (11) to the data the following function proposed in Connolly et al. (2009) were used:

$$n_{\mathrm{s}}(T) = \begin{cases} a_1(T + a_2)^2, & T < a_2 \\ 0, & T \geq a_2 \end{cases} \tag{12}$$

4.4 Comparison of the models

Applying the four models described in Sects. 4.2 and 4.3 to the experimental data we obtained the fit curves shown in Fig. 7. Best fit parameters obtained by the least square method are given in Table 2. The two models that combine a stochastic formation of the ice embryo with a distribution of surface properties (α-pdf and active site model) also referred to as modified singular models (e.g., Vali, 2008), represent the experimental data best. The α-pdf model represents the measurements slightly better than the active site model. This might indicate a relatively large variety of characteristics between individual particles rather than many diverse active sites on a given particle. Time dependence is less pronounced in the α-pdf than in the active site model.

Also the singular approach adequately reproduces the frozen fraction within the 21 s of the experiment, but is unable to capture the observed increase in frozen fraction with

ACPD
12, 12623–12662, 2012

time. Both active site models (singular and stochastic active site model) over predict the influence of the particle surface on freezing temperatures (q.v. Sect. 6.2). This however might also indicate an insufficient representation of the surface available for nucleation in the formulas used in this study. A stochastic fit to the measurements using a single contact angle is neither able to capture the time nor temperature dependence in an adequate manner.

5 Atmospheric implication

To illustrate the difference in the predicted frozen fraction from different physical descriptions of the particle surface (single contact angle, α-pdf, active sites) and germ formation process (stochastic, singular) we calculated the time evolution of a mixed-phase cloud and the dependence of the medium freezing temperature on the size of the particles. In these two applications, the importance of an appropriate description of ice nucleation in predicting ice formation becomes particularly apparent.

5.1 Glaciation time of an isothermal water cloud

Supercooled clouds have a finite lifetime in which ice nucleation can take place. To provide some information on the natural conditions for which the reported measurements are relevant, we used the four freezing models to extrapolate the freezing state of an isothermal cloud to an atmospheric timescale. We estimated the available glaciation time to be on the order of the timescale over which the Bergeron-Findeisen process would consume the liquid water content of a cloud consisting of 50 % ice crystals and

ACPD
12, 12623–12662, 2012

50 % droplets of 5 µm radius, i.e.

$$\frac{\mathrm{d}r_{\mathrm{drop}}^2(t)}{\mathrm{d}t} = \underbrace{V_{\mathrm{H_2O}} \cdot D_g(T) \cdot \left(\frac{p_{\mathrm{i}}(T) - p_{\mathrm{w}}(T)}{RT}\right)}_{c} \tag{13}$$

$$\tau = \frac{r_{\mathrm{drop}}^2(t=0)}{c} \tag{14}$$

where r_{drop} denotes the radius of the liquid drop, $V_{\mathrm{H_2O}}$ the volume of a water molecule, $D_g(T)$ the temperature dependent water vapour diffusion coefficient, and p_{i}, p_{w} the saturation vapour pressure over ice and water, respectively. The cloud lifetime τ has been estimated to be on the order of 30 min. Using τ as a representative time scale available for ice nucleation in a mixed phase cloud, the importance of time on the glaciation state becomes explicit. By applying the four different model approaches described previously, we calculate the time evolution of the frozen fraction over 30 min. It can be seen from Fig. 8 that the choice of an accurate approach is fundamental to describe the glaciation of a mixed-phase cloud. The simple stochastic model is highly sensitive to the particle size, temperature and time. Taking into account a spectrum of contact angles as was done with the α-pdf and active site model, lowers the dependence on temperature and time compared to the stochastic model. The influence of particle size on the α-pdf model is a proportional shift to higher frozen fractions with increasing IN radius. Compared to the α-pdf, the active site model predicts a steeper time dependence and increase of the frozen fraction for larger particle surface.

The rapid change in the frozen fraction for increasing residence time, calculated for the active site model is unexpected, as this model, although also based on CNT, is conceptionally closer to the singular model than the α-pdf or the stochastic model. Probably the assumption of a 6 nm^2 active site area (Lüönd et al., 2010) and the resulting number of active sites generated per particle is too high (i.e. 335 167 active sites on a 800 nm particle). Combined with the steep increase of the surface density function (Eq. 8), this might cause the particle population to appear too homogeneous i.e. little

ACPD
12, 12623–12662, 2012

variation of the best active site present on a particle among the particle population. As preferentially the best active sites initiate freezing, the resulting time-dependent fit curves of the active sites model seems to resemble a stochastic nucleation which takes place on a single active site surface exhibiting an efficient contact angle.

By assuming a log-normal size distribution of the particles, we tested if the time dependence would be decreased by the variable activity of the different particle sizes. It can be seen in the lowest row of Fig. 8 that the size distribution causes the slope in the active site model to increase stronger in the beginning (resembling the stochastic freezing curve) and flattening out after a relatively short time. This indicates that a fraction of the larger particles has a high probability to host an efficient active site, that causes these particles to activate rapidly, whereas the fraction of smaller particles activates at a delay. The faster increase in frozen fraction of larger particles can also be seen when comparing the freezing curves for the mono disperse 400 nm and 800 nm particles. A bimodal size distribution i.e. a distribution with a second peak at larger sizes, might cause an even steeper increase in the beginning followed by a weak, flattening slope. Though being stochastic in nature, the initial rapid freezing of a fraction of droplets containing the larger aerosol mode followed by little additional freezing initiated by the smaller mode, could mimic a singular ice nucleation behaviour. As can be seen in the forth column of Fig. 8 for the singular, polydisperse case a reduction in the temperature dependence of the frozen fraction is predicted. The influence of the particle size distribution becomes important as the threshold temperature where a particle can serve as IN i.e. the occurrence of a site, active at that specific temperature, is proportional to the particle surface area. A size distribution therefore results in a higher frozen fraction even at high temperatures, due to the activation of large IN and a lower activation at lower temperatures in comparison to a mono disperse aerosol population.

ACPD
12, 12623–12662, 2012

6 Discussion and limitations

Scanning electron microscope (SEM) pictures of the kaolinite sample (Fluka) used in this study can be found in Welti et al. (2009) and Ladino et al. (2011). The kaolinite particles are not spherical and exhibit rugged, stratified surfaces. Therefore, results for size selected particles are likely to represent a lower limit of the surface area of the particles used in this study. The geometric surface area was used instead of an approximately 2 to 4 times larger N_2 Brunauer-Emmett-Teller (BET) surface area as reported for example in Murray et al. (2011). Due to the larger size of water molecules and the partly hydrophobic property of the mineral dust surface, the area where water can adsorb on a particle can be expected to be smaller than the surface occupied by nitrogen molecules (Zettlemoyer et al., 1961).

The freezing efficiency of kaolinite is known to differ for samples from different sources. The kaolinite (Fluka) used in this study is known to be a relatively efficient IN (Pinti et al., 2012). Also the observable time dependence of the frozen fraction would be distinctly different for different IN, as can be already seen in the variance between the two tested particle sizes. The IN activity could also be an impermanent feature, as from the moment the aerosols are released into the atmosphere until they become active in clouds they are exposed to sunlight and chemical compounds in the air that might lead to loss or increase of their nucleation activity, therefore the time dependence of nucleation on a single species could change with aging-time.

The different approaches to compute the frozen fraction with fit parameters gained from the measurements yield different dependencies on nucleation time. Using a time-dependent, stochastic description of the nucleation mechanism in combination with the pdf-contact angle distribution leads to the best agreement with the experimental data. Therefore we recommend to include a time-dependence in numerical calculations of the evolution of mixed-phase clouds. To compare the effect of time and temperature on the frozen fraction of immersion freezing on the kaolinite dust investigated in this study, we refer to the α-pdf and active sites fit curves shown in Fig. 8, at a typical mixed-

ACPD
12, 12623–12662, 2012

phase cloud temperature of 243 K. A change in time scale by a factor of 10 results in approximately the same increase in frozen fraction as a shift in temperature by 1 K. A small change in supercooling will therefore cause a much larger change in the frozen fraction than a change in the nucleation time. This implies that temperature is more important than time in determining immersion freezing. This is in agreement with the findings of Vali (2008).

6.1 Temperature dependent, apparent contact angle

In CNT, the contact angle is usually assumed to be a constant which depends only on the properties of the substrate on which nucleation is initiated. Using Eqs. (1)–(3) and the stochastic model (Eq. 5) we calculated the contact angle as a function of temperature for each individual experiment. The resulting contact angles are given in Fig. 9. Calculating the apparent contact angle of each individual measurement with CNT revealed a nearly linear relationship of the contact angle with temperature. This temperature dependence represents the deviations of the experimental results from the predictions of the stochastic model. The decrease in contact angle with increasing temperature reflects an increase of the importance of the geometric factor f to the Gibbs free energy for nucleation. The particle surface lowers the energy barrier of germ formation at higher temperatures whereas the contribution of the surface decreases towards homogeneous freezing temperatures.

Particles with small contact angles are able to initiate nucleation at higher temperatures than particles with larger contact angles. α(T) reflects the mean active contact angle at a certain temperature without giving information about how the contact angles are distributed among the particles. Alpert et al. (2011) pointed out that according to Young's equation (Pruppacher and Klett, 1997) a temperature dependence of contact angle α could be expected due to the temperature dependence of the surface tensions between the substrate, water and ice phase. The Young equation gives the relation be-

ACPD
12, 12623–12662, 2012

tween contact angle of immersion freezing and the thereby involved surface tensions:

$$\cos(\alpha(T)) = \frac{\sigma_{s/a}(T) - \sigma_{s/i}(T)}{\sigma_{i/w}(T)} \quad (15)$$

here $\alpha(T)$ is the contact angle and $\sigma_{s/a}(T)$, $\sigma_{s/i}(T)$, $\sigma_{i/w}(T)$ the temperature dependent surface tensions between the kaolinite surface and water, the surface and ice, and between ice and water, respectively. By using the temperature dependent mean contact angle, a value for $\sigma_{s/a}$ reported in Helmy et al. (2004) and the parametrisation of $\sigma_{i/w}(T)$ which can be found in Pruppacher and Klett (1997) the surface tension between the ice germ and the kaolinite substrate ($\sigma_{s/i}$) can be derived. We find reasonable values of $\sigma_{s/i}$ (243 K) $\approx 0.078\,\mathrm{J\,m^{-2}}$ increasing by $0.0013\,\mathrm{J\,m^{-2}\,K^{-1}}$ towards lower temperatures. This test confirms that it is plausible to attribute a change in contact angle to a change in surface tension with temperature. However, to conclude on the physical meaning of this finding, is out of scope of this study.

We conclude, that as particles with high contact angles become active at lower temperatures the average active contact angle of a population could be parameterised as temperature dependent within the stochastic model. This might be a simple way to parameterize immersion freezing in climate models without applying calculation intense surface parameterisations.

6.2 Surface area dependence of the mean freezing temperature

A comparison of the surface area dependent median freezing temperature (50 % of drops unfrozen) obtained from the four previously described models and from the temperature dependent contact angle parametrisation, revealed a large variation in the prediction of the particle surface area required to freeze 50 % of a droplet population. Measurements of droplets containing several particles as done e.g. in DSC studies, could provide information on the surface dependent median freezing temperature for larger available surface areas. This information could be of value for modelling stud-

ACPD
12, 12623–12662, 2012

ies e.g., Diehl and Wurzler (2004) and Lohmann and Diehl (2006) have used median freezing temperatures to compute droplet freezing rates in their climate models.

7 Conclusions

The ability of kaolinite particles to act as IN under mixed phase cloud condition and the importance of nucleation time have been investigated in the immersion mode.

A dependence of the frozen fraction from immersion freezing on time has been observed. This confirms that immersion freezing is at least partly a stochastic phenomenon. For the atmosphere this means that the droplets of a supercooled cloud continue to transform to ice even without further cooling. This has been observed in static supercooled clouds which persist for hours (Westbrook and Illingworth, 2009).

Because larger particles have a larger contact area to the liquid phase or a higher probability of carrying efficient nucleation sites, the minimum supercooling to activate them as IN is smaller than for smaller particles. Beside the particle size, the temperature has a strong influence on the time required for droplets to freeze. The exponential dependence of the nucleation rate on temperature in the framework of CNT, indicates that there is virtually no freezing above a certain temperature, except for very long lived clouds or huge particles. The experiments reported here, show that smaller particles need more time to nucleate ice at a given temperature than larger particles i.e. the influence of time on the frozen fraction is stronger the smaller the particles are and becomes most evident at the onset temperature of immersion freezing. Similar conclusions have been reached for AgI particles by Vonnegut (1949) and Gerber (1976).

It follows that measurements of the concentrations of particles able to act as IN in a particular experiment or atmospheric process have to be qualified with respect to the particle size and both the available time to freeze and the temperature, as has been called for before, e.g. by Vonnegut (1987).

We used time-dependent and one time-independent model to investigate their applicability to describe the measured frozen fraction from the experiment. The models

ACPD
12, 12623–12662, 2012

yield essential variances. A purely stochastic model diverges substantially from the measurement. It over predicts the time evolution as well as the temperature dependence of immersion freezing. The singular model is able to fit the frozen fraction in the limited nucleation time but over predicts the effect of particle size on the temperature of freezing. Modified stochastic models (α-pdf and active site) capture the temperature and time-dependent ice fraction well. However, revised contact angle distribution functions might benefit the model accuracy. However, the lack of knowledge on the correlation between the surface structure and the nucleation ability makes it difficult to find an appropriate description on a microscopic scale. E.g. the function by which the active site density is described in the active site model might look completely different. If active sites were distributed over the range of contact angles according to a bimodal distribution with two distinctly separated maxima, e.g. due to the presence of two different properties that aid nucleation, time dependence would be masked by rapid activation of particles with the efficient property and extremely slow activation of particles with the inefficient one. The resulting evolution in time at a constant temperature would mimic singular behaviour. Generally a wide distribution of properties (surface area or chemical) among particles found in a cloud might create a more singular freezing behaviour than a narrow distribution around the same average.

To definitively conclude whether single active sites or the surface structure of the entire IN are responsible for immersion freezing is not possible based on the data available in this study. The fact that the nucleation activity can be described appropriately by assuming a contact angle distribution over the whole particle ensemble might indicate that average properties are better suited for parameterisations. To further investigate if there are active sites or more uniformly distributed properties that are responsible for the nucleation process, the effect of surface area could be studied for a large range of particle diameters (10 nm–10 µm). Such dataset would allow to test the dependency predicted by the two approaches (shown in Fig. 10).

A combination of a less broad distribution of contact angles than reported in Sect. 4 among an ensemble of particle together with a temperature dependence (for example

ACPD
12, 12623–12662, 2012

of $\sim 2^{\circ}\,K^{-1}$ or as an additional free parameter) could be tested to take into account the temperature dependence of contact angles in combination with a contact angle distribution.

Acknowledgements. We acknowledge financial support from the Swiss National Funds (SNF).

References

Alpert, P., Aller, J., and Knopf, D.: Initiation of the ice phase by marine biogenic surfaces in supersaturated gas and supercooled aqueous phases, Phys. Chem. Chem. Phys., 13, 19882–19894, doi:10.1039/c1cp21844a, 2011. 12643

Barnes, G. T., Katz, U., and Sänger, R.: Ice forming activity and the surface properties of nucleating materials, Z. Angew. Math. Phys., 13, 76–80, 1962. 12634

Bigg, E.: The supercooling of water, P. Phys. Soc. London B, 66, 688–694, 1953. 12626, 12634

Broadley, S. L., Murray, B. J., Herbert, R. J., Atkinson, J. D., Dobbie, S., Malkin, T. L., Condliffe, E., and Neve, L.: Immersion mode heterogeneous ice nucleation by an illite rich powder representative of atmospheric mineral dust, Atmos. Chem. Phys., 12, 287–307, doi:10.5194/acp-12-287-2012, 2012. 12627

Cantrell, W. and Heymsfield, A.: Production of ice in tropospheric clouds, B. Am. Meteorol. Soc., BAMS-86-6-795, 795–806, 2005. 12625

Chakraverty, B. and Pound, G.: Heterogeneous nucleation at macroscopic steps, Acta Metall. Mater., 12, 851–860, 1964. 12635

Connolly, P. J., Möhler, O., Field, P. R., Saathoff, H., Burgess, R., Choularton, T., and Gallagher, M.: Studies of heterogeneous freezing by three different desert dust samples, Atmos. Chem. Phys., 9, 2805–2824, doi:10.5194/acp-9-2805-2009, 2009. 12627, 12638

DeMott, P., Sassen, K., Poellot, M., Baumgardner, D., Rogers, D., Brooks, S., Prenni, A., and S. M., K.: African dust aerosols as atmospheric ice nuclei, Geophys. Res. Lett., 30, 1732, doi:10.1029/2003GL017410, 2003. 12624

Diehl, K. and Wurzler, S.: Heterogeneous drop freezing in the immersion mode: model calculations considering soluble and insoluble particles in the drops, J. Atmos. Sci., 61, 2063–272, 2004. 12645

ACPD

12, 12623–12662, 2012

Eastwood, M., Cremel, S., Gehrke, C., Girard, E., and Bertram, A. K.: Ice nucleation on mineral dust particles: onset conditions, nucleation rates and contact angles, J. Geophys. Res., 113, D22203, doi:10.1029/2008JD010639, 2008. 12624
Fletcher, N.: On ice-crystal production by aerosol particles, J. Meteorol., 16, 173–180, 1959. 12626
Fletcher, N.: Active sites and ice crystal nucleation, J. Atmos. Sci., 26, 1266–1271, 1969. 12634
Gerber, H.: Relation of size and activity of AgI smoke particles, J. Atmos. Sci., 33, 667–677, 1976. 12633, 12645
Helmy, A. K., Ferreiro, E. A., and de Bussetti, S. G.: The surface energy of kaolinite, Colloid Polym. Sci., 283, 225–228, 2004. 12644
Hoose, C., Kristjánsson, J., Chen, J., and Hazra, A.: A classical-theory-based parameterization of heterogeneous ice nucleation by mineral dust, soot, and biological particles in a global climate model, J. Atmos. Sci., 67, 2483–2503, 2010. 12633
Houghton, H. G.: A preliminary quantitative analysis of precipitation mechanisms, J. Meteorol., 7, 363–369, 1950. 12625
Isono, K., Komabayasi, M., and Ono, A.: The nature and origin of ice nuclei in the atmosphere, J. Meteorol. Soc. Jpn., 37, 211–233, 1959. 12624
Koop, T.: Homogeneous ice nucleation in water and aqueous solutions, Z. Phys. Chem., 218, 1231–1258, 2004. 12627
Kumai, M.: Electron-microscope study of snow-crystal nuclei, J. Atmos. Sci., 8, 151–156, 1951. 12624
Ladino, L., Stetzer, O., Lüönd, F., Welti, A., and Lohmann, U.: Contact freezing experiments of kaolinite particles with cloud droplets, J. Geophys. Res., 116, D22202, doi:10.1029/2011JD015727, 2011. 12642
Langham, E. and Mason, B.: The heterogeneous and homogeneous nucleation of supercooled water, P. R. Soc. A, 247, 493–504, 1958. 12626
Lüönd, F., Stetzer, O., Welti, A., and Lohmann, U.: Experimental study on the ice nucleation ability of size-selected kaolinite particles in the immersion mode, J. Geophys. Res., 115, D14201, doi:10.1029/2009JD012959, 2010. 12627, 12628, 12630, 12631, 12634, 12637, 12640, 12657
Lohmann, U.: A glaciation indirect aerosol effect caused by soot aerosols, Geophys. Res. Lett., 29, 1052, doi:10.1029/2001GL014357, 2002. 12625

ACPD
12, 12623–12662, 2012

Lohmann, U. and Diehl, K.: Sensitivity studies of the importance of dust ice nucleation for the indirect aerosol effect on stratiform mixed-phase clouds, J. Atmos. Sci., 63, 968–982, 2006. 12645

Marcolli, C., Gedamke, S., Peter, T., and Zobrist, B.: Efficiency of immersion mode ice nucleation on surrogates of mineral dust, Atmos. Chem. Phys., 7, 5081–5091, doi:10.5194/acp-7-5081-2007, 2007. 12627, 12637

Murray, B. J., Broadley, S. L., Wilson, T. W., Atkinson, J. D., and Wills, R. H.: Heterogeneous freezing of water droplets containing kaolinite particles, Atmos. Chem. Phys., 11, 4191–4207, doi:10.5194/acp-11-4191-2011, 2011. 12627, 12642

Nicolet, M., Stetzer, O., Lüönd, F., Möhler, O., and Lohmann, U.: Single ice crystal measurements during nucleation experiments with the depolarization detector IODE, Atmos. Chem. Phys., 10, 313–325, doi:10.5194/acp-10-313-2010, 2010. 12628, 12631

Niedermeier, D., Shaw, R. A., Hartmann, S., Wex, H., Clauss, T., Voigtländer, J., and Stratmann, F.: Heterogeneous ice nucleation: exploring the transition from stochastic to singular freezing behavior, Atmos. Chem. Phys., 11, 8767–8775, doi:10.5194/acp-11-8767-2011, 2011. 12627

Pinti, V., Marcolli, C., Zobrist, B., Hoyle, C. R., and Peter, T.: Ice nucleation efficiency of clay minerals in the immersion mode, Atmos. Chem. Phys. Discuss., 12, 3213–3261, doi:10.5194/acpd-12-3213-2012, 2012. 12627, 12642

Pruppacher, H. and Klett, J.: Microphysics of clouds and precipitation, Springer Netherlands, Dordrecht, The Netherlands, doi:10.1007/978-0-306-48100-0, 1997. 12625, 12629, 12635, 12643, 12644

Rogers, D.: Development of a continuous flow thermal gradient diffusion chamber for ice nucleation studies, Atmos. Res., 22, 149–181, 1988. 12628

Shaw, R., Durant, A., and Mi, Y.: Heterogeneous surface crystallization observed in undercooled water, J. Phys. Chem. B, 109, 9865–9868, doi:10.1021/jp0506336, 2005. 12627

Stetzer, O., Baschek, B., Luond, F., and Lohmann, U.: The Zurich Ice Nucleation Chamber (ZINC) – a new instrument to investigate atmospheric ice formation, Aerosol Sci. Tech., 42, 64–74, 2008. 12628, 12630

Tabazadeh, A., Djikaev, Y. S., and Reiss, H.: Surface crystallization of supercooled water in clouds, P. Natl. Acad. Sci. USA, 99, 15873–15878, doi:10.1073/pnas.252640699, 2002. 12625

Vali, G.: Atmospheric ice nucleation – A review, J. Rech. Atmos., 19, 105–115, 1985. 12625

ACPD

12, 12623–12662, 2012

Vali, G.: Repeatability and randomness in heterogeneous freezing nucleation, Atmos. Chem. Phys., 8, 5017–5031, doi:10.5194/acp-8-5017-2008, 2008. 12627, 12638, 12643
Vali, G. and Stansbury, E.: Time-dependent characteristics of the heterogeneous nucleation of ice, Can. J. Phys., 44, 477–502, 1966. 12627
Vonnegut, B.: Nucleation of supercooled water clouds by silver iodide smokes, Chem. Rev., 44, 277–289, 1949. 12626, 12645
Vonnegut, B.: Importance of including time in the specification of ice nucleus concentration, J. Clim. Appl. Meteorol., 26, p. 322, 1987. 12645
Wang, Z., Zhang, D., and Deng, M.: A global view of mixed-phase cloud distribution and ice generation in them with A-train satellite measurements, in: 13th Conference on Cloud Physics, Abstract No. 12.6, 28 June–2 July 2010, Portland, Oregon, USA, 2010. 12625
Wartburton, J. and Heffernan, K.: Time lag in ice crystal nucleation by silver iodide, J. Appl. Meteorol., 3, 788–791, 1964. 12626
Welti, A., Lüönd, F., Stetzer, O., and Lohmann, U.: Influence of particle size on the ice nucleating ability of mineral dusts, Atmos. Chem. Phys., 9, 6705–6715, doi:10.5194/acp-9-6705-2009, 2009. 12629, 12642
Westbrook, C. and Illingworth, A.: Stochastic ice nucleation in supercooled clouds, and constraints on the fraction of small ice crystals in glaciated clouds, observed using Doppler lidar and radar, in: 8th ISTP, Article No.: S01-O02 19–23 October 2009, Delft, The Netherlands, 2009. 12625, 12645
Zettlemoyer, A., Tcheurekdjian, N., and Chessick, J.: Surface properties of silver iodide, Nature, 18, p. 653, doi:10.1038/192653a0, 1961. 12642
Zobrist, B., Koop, T., Luo, B. P., Marcolli, C., and Peter, T.: Heterogeneous ice nucleation rate coefficient of water droplets coated by a nonadecanol monolayer, J. Phys. Chem. C, 111, 2149–2155, 2007. 12627, 12635

ACPD
12, 12623–12662, 2012

Table 1. Residence time in ZINC before the frozen fraction was detected in dependence of position of detection and total flow.

Flow	Position 1	Position 2	Position 3	Position 4
19 l min^{-1}	1.1 s	2.3 s	–	–
10 l min^{-1}	3.0 s	5.9 s	8.9 s	10.3 s
5 l min^{-1}	–	–	–	21.4 s

ACPD
12, 12623–12662, 2012

Table 2. Fit parameters obtained for the four models described in Sects. 4.2 and 4.3. The root mean square errors (RMSE) between the fit curves and the data are given in the last column.

Model	Parameter	Value	RMSE
Stochastic	α	90.75°	0.242
α-pdf	μ	91.94°	0.111
	σ	0.0942	
Active sites	b	$4.550 \times 10^{13}\,\mathrm{m}^{-2}$	0.127
	β_1	12.39°	
	β_2	64.66°	
Singular	a_1	$8.569 \times 10^{10}\,\mathrm{m}^{-2}\,\mathrm{K}^{-2}$	0.156
	a_2	242.65 K	

ACPD
12, 12623–12662, 2012

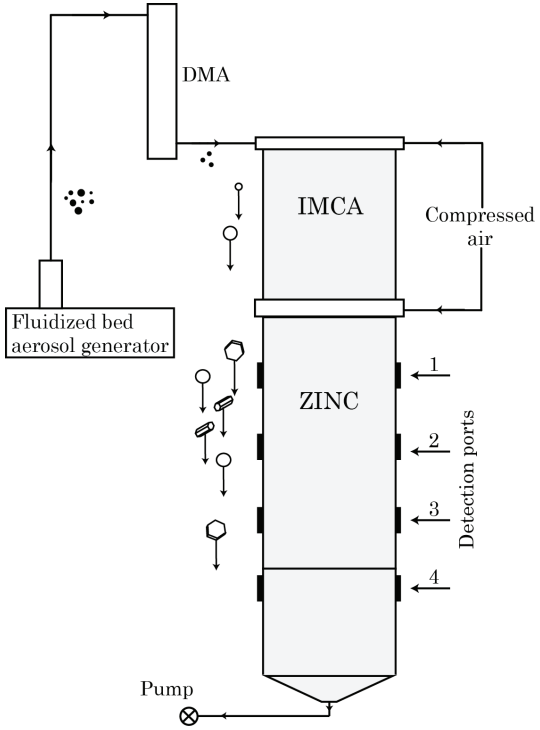

Fig. 1. Schematic of the experimental setup. A fluidized bed aerosol generator is used to produce mineral dust aerosol. Particles with 400 nm and 800 nm diameter are selected with a DMA. In the top of IMCA particles activate as CCN at 300 K before they are continuously cooled down to the freezing temperature prevailing in ZINC. In the transition from IMCA to ZINC additional sheath air is introduced to counteract buoyant displacement of the droplets from the centre position. In ZINC the droplets are exposed to cold temperatures and eventually the immersed particles cause the droplets to freeze. The time-dependent frozen fraction is detected with IODE consecutively at the four detection ports.

ACPD
12, 12623–12662, 2012

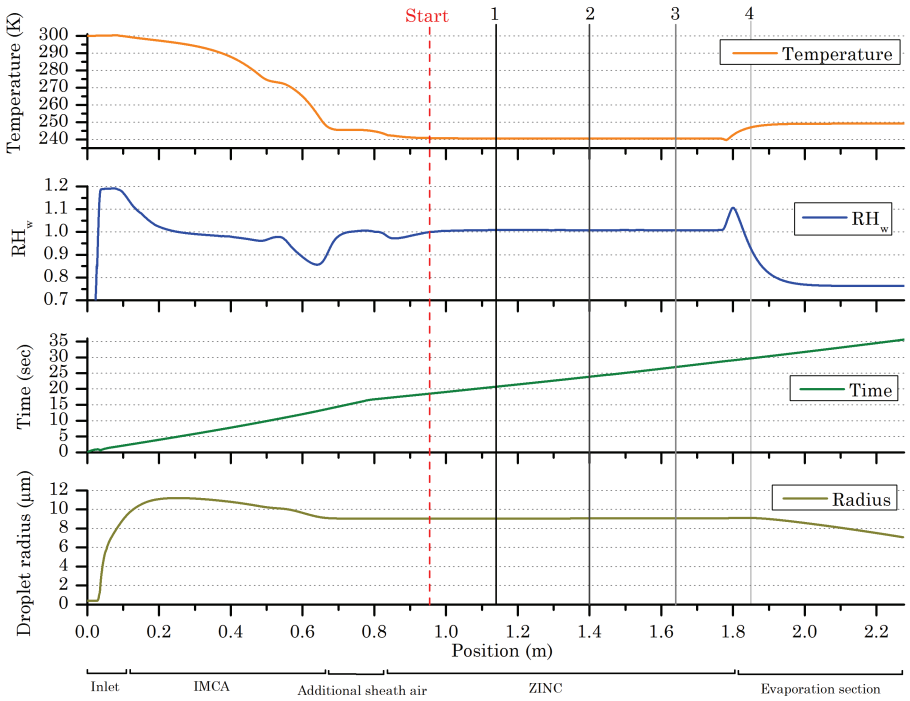

Fig. 2. Experimental conditions along a particle trajectory in the sample air. From top to down the air temperature, relative humidity with respect to water, residence time and calculated droplet size are shown with respect to the vertical location in the experiment. The corresponding parts are labeled at the bottom. The vertical red line indicates the position from where nucleation time was counted. Vertical grey lines numbered with 1–4 show the positions of detection of the frozen fraction.

ACPD
12, 12623–12662, 2012

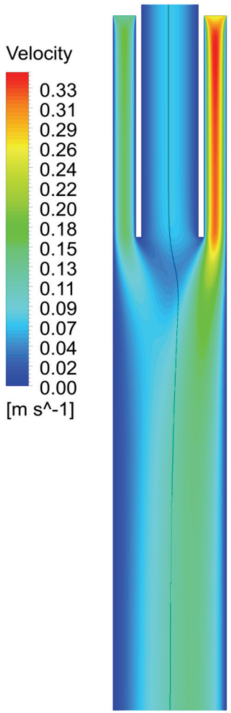

Fig. 3. Flow velocity in the additional sheath air. The additional flow is adjusted to counteract the buoyant displacement of the aerosol layer, depending on ΔT between the cold and the warm wall in ZINC. The black line indicates an example particle trajectory.

ACPD
12, 12623–12662, 2012

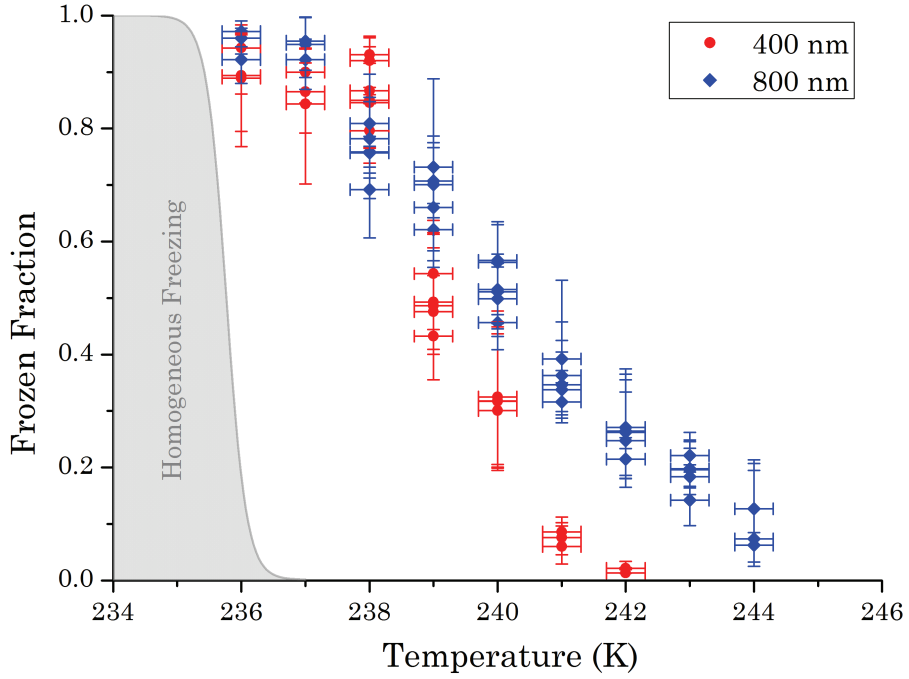

Fig. 4. Temperature dependent frozen fraction of 400 nm and 800 nm kaolinite particles for a residence time of 9 s. Homogeneous freezing conditions are shaded in grey.

ACPD
12, 12623–12662, 2012

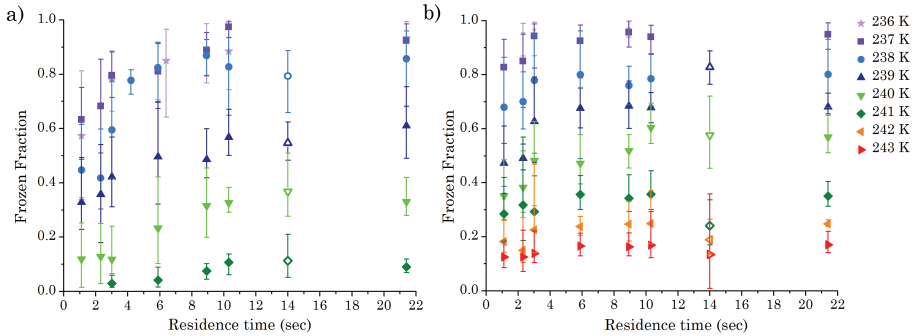

Fig. 5. Time dependent frozen fraction in the immersion mode for temperatures between 236 K and 243 K. Each point represents an average of 3 to 7 measurements. **(a)** shows the results for size selected 400 nm kaolinite particles and **(b)** 800 nm kaolinite particles. For comparison, results reported in Lüönd et al. (2010) are shown as open symbols.

ACPD
12, 12623–12662, 2012

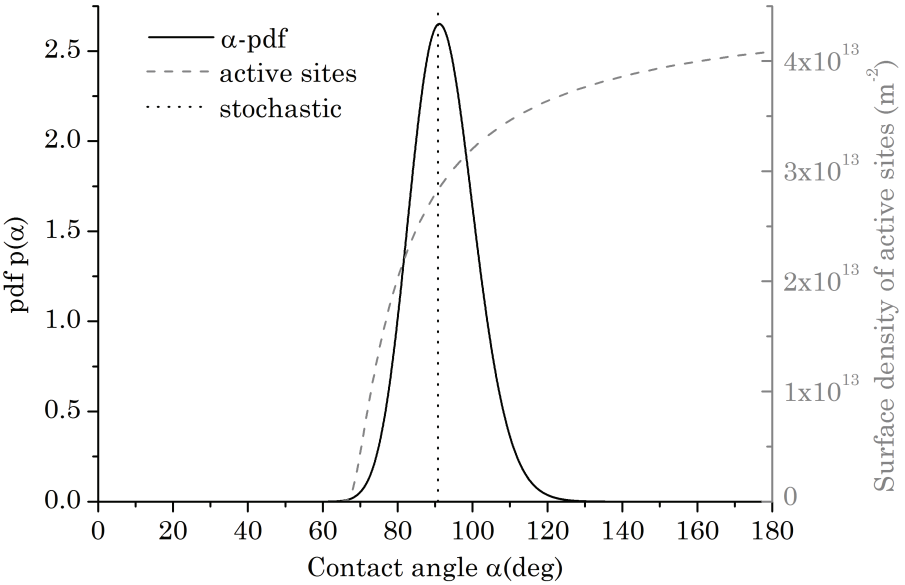

Fig. 6. Contact angle distribution on the particles.

ACPD
12, 12623–12662, 2012

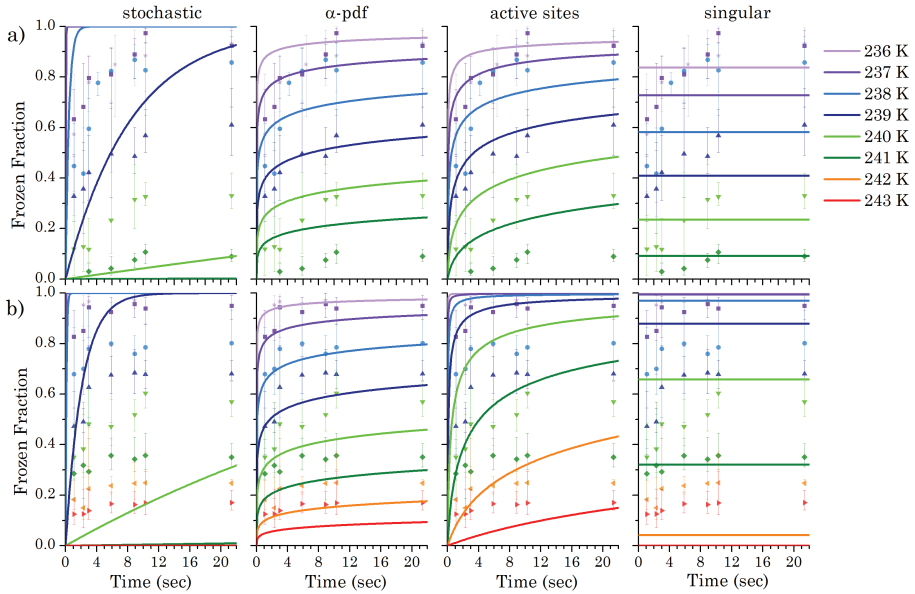

Fig. 7. Comparison of the fit curves obtained with the four models with experimental data. **(a)** 400 nm kaolinite particles. **(b)** 800 nm kaolinite particles. The parameters used to obtain the fit curves for both particle sizes are given in Table 2. The error bars represent the uncertainty in the distinction between water and ice.

ACPD
12, 12623–12662, 2012

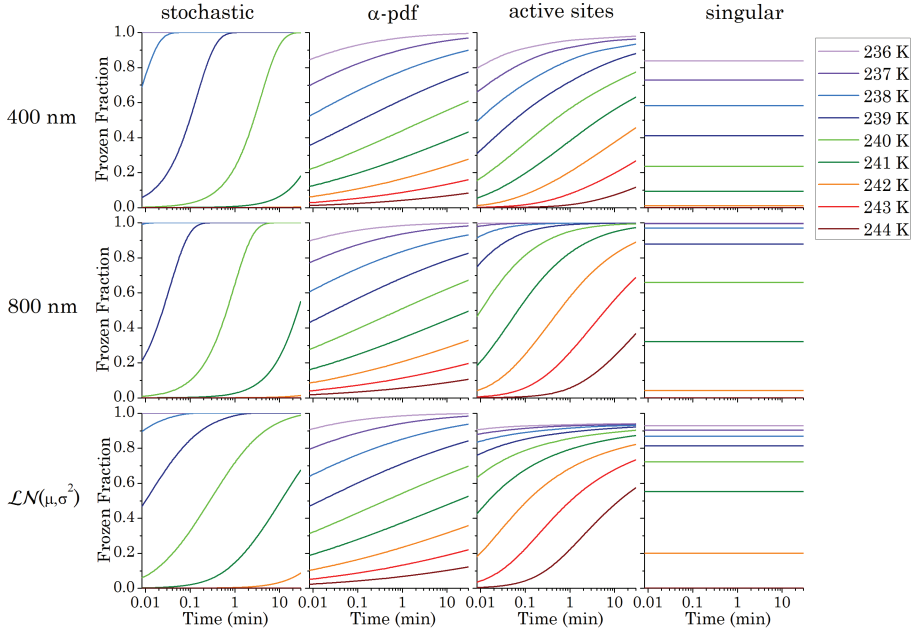

Fig. 8. Calculated increase in the frozen fraction with time for 400 nm, 800 nm mono disperse particles and for a particle ensemble exhibiting a log-normal size distribution with μ = 600 nm and σ^2 = 1. The fitting parameters obtained in Sect. 4.1 for the four different models are applied to calculate a 30 min time evolution of the frozen fraction at temperatures between 236 K to 244 K.

ACPD
12, 12623–12662, 2012

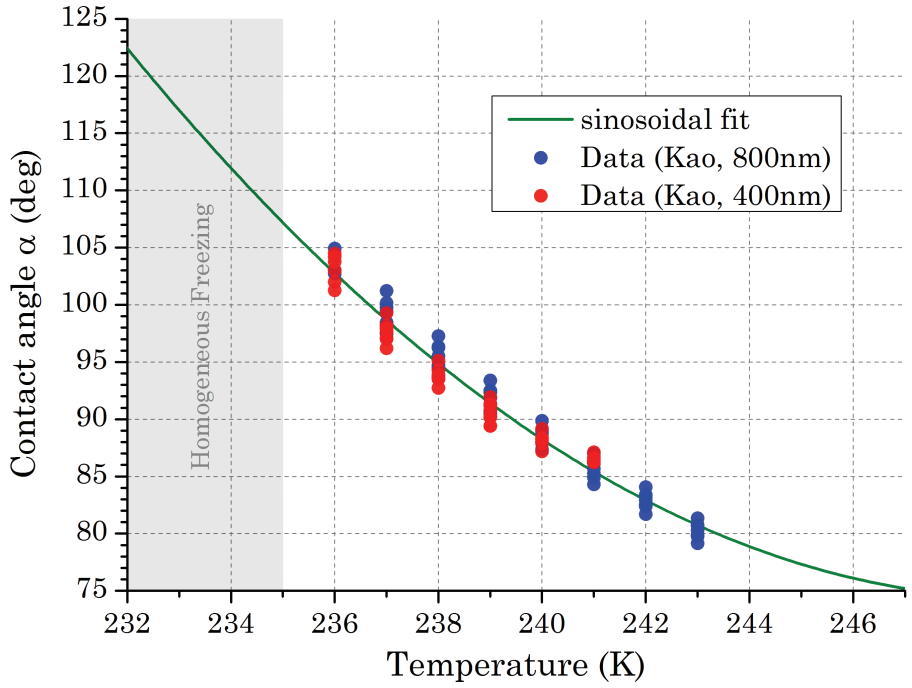

Fig. 9. Contact angle vs. temperature for 400 nm and 800 nm kaolinite particles in the immersion mode. Calculated using classical nucleation theory.

ACPD
12, 12623–12662, 2012

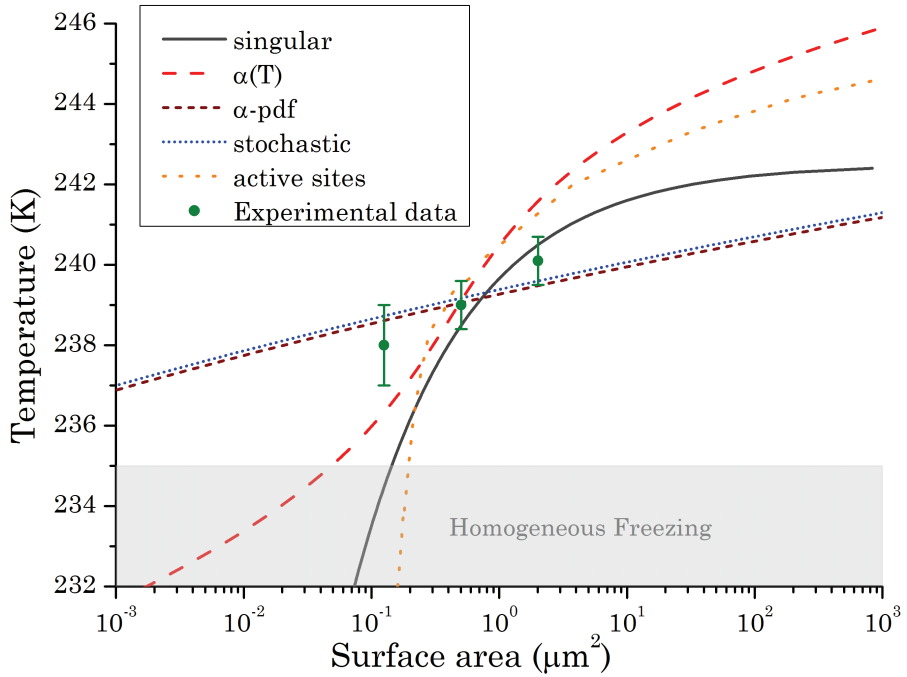

Fig. 10. Surface area dependent median freezing temperature i.e. temperature at which a kaolinite particle with the corresponding surface area will nucleate ice in immersion mode with a probability of 50 %. In a population of droplets this corresponds to 50 % frozen droplets. Nucleation time is 10 s.

ACPD
12, 12623–12662, 2012